INTERNATIONAL JOURNAL FOR NUMERICAL METHODS IN FLUIDS
Int. J. Numer. Meth. Fluids 2003; **43**:165–181 (DOI: 10.1002/fld.602)

Numerical analysis of supersonic combustion ramjet with upstream fuel injection

Raffaele Savino*,† and Giuseppe Pezzella

Dipartimento di Scienza e Ingegneria dello Spazio "Luigi G. Napolitano" (DISIS), Università di Napoli "Federico II", P.le Tecchio 80, Naples, Italy

SUMMARY

This paper describes possible fuel injection scheme for airbreathing engines that use hydrocarbon fuels. The basic idea is to inject fuel at the spike tip of the supersonic inlet to achieve mixing and combustion efficiency with a limited length combustion chamber. A numerical code, able to solve the full Navier–Stokes equations in turbulent and reacting flows, is employed to obtain numerical simulations of the thermo-fluidynamic fields at different scramjet flight conditions, at Mach numbers of $M = 6.5$ and 8. The feasibility of the idea of the upstream injection is checked for a simple axisymmetric configuration and relatively small size.

The results are discussed in connection with the potential benefits deriving from the use of new ultra high temperature ceramics (UHTC). Copyright © 2003 John Wiley & Sons, Ltd.

KEY WORDS: ramjet; scramjet; numerical analysis; ultra high temperature ceramics

INTRODUCTION

The exploitation of a supersonic combustion ramjet engine for various high-speed applications has been a dream for many years. The feasibility of hypersonic air breathing engines has been and is the subject of many research programmes in the United States, Russia, Europe and Japan [1].

Starting with the pioneering work by Ferri [2] at the Aerodynamics Laboratory of the Polytechnic Institute of Brooklyn (PIBAL) and at General Applied Science Laboratories (GASL), scramjet engines research has continuously attracted interest of the aerospace community for the different hypersonic applications (missiles, hypersonic cruise missions, single-stage to-orbit (SSTO) and two-stage-to-orbit (TSTO), space planes, reusable launch vehicles, etc.).

Technology readiness of the air breathing propulsion system (i.e. the scramjet) in flight is a major challenge that hinders the application of scramjets. In recognition of this and

*Correspondence to: R. Savino, Dipartimento di Scienza e Ingegnaria della Spazio "Luigi G. Napolitano" (DSIS), Università di Napoli "Federico II", P.le Tecchio 80, Naples, Italy.
†E-mail: raffaele.savino@unina.it

Received 9 November 2002
Revised 20 March 2003

other challenges NASA's Advanced Transportation Programme foresees research and technologies development in hypersonic and propulsion as the preconditions to reach the goal of reducing the cost per pound of payload to LEO to $100 by year 2025. Very recently NASA has announced a project (X-43C) to flight test a hydrocarbon-fuelled (JP-7) scramjet engine developed by the U.S. Air Force.

Scramjet research programmes are in progress in Japan (at NAL), France (at Onera), Germany (at DLR), India and in China.

One of the main drawbacks of the scramjet is that, for flight Mach number above 6, achieving complete mixing and combustion in a supersonic stream in a limited size combustion chamber has proven to be a very difficult problem. One concept to improve the mixing and combustion efficiencies in scramjets is to produce a premixed fuel–air mixture (at a suitable Mach number higher than one) with minimum losses and drag. Different concepts of fuel–air mixing enhancement at the entrance of a supersonic combustor have been investigated [3]; mixing enhancement over short axial distances relies on the formation of vortical or separated flows. However, this leads to substantial total pressure losses. Typical fuel injection and mixing schemes for supersonic combustors include normal and angled injection from the flow channel wall or from in-stream pylon walls, coflowing (axial injection from the base of reverse steps) or combinations of these [3, 4]. In many cases these systems require large supply pressures and, in addition, cause additional total pressure losses, aerodynamic drag and construction complexity (e.g. active cooling requirements).

One way to overcome these problems is to investigate an idea proposed forty years ago [5] that consists of injecting fuel at the supersonic inlet tip to promote mixing before the air stream reaches the combustion chamber. In this way it is possible to take advantage of the temperature and pressure conditions behind the upstream shock waves to increase the mixing efficiency, obtaining a hot air/fuel mixture at the beginning of the combustor and reducing the times for ignition and combustion to values of the same order of magnitude as the mixture residence time inside the 'short' combustor. This scheme of fuel injection upstream of the combustion chamber has therefore two main advantages: (1) premixing the fuel–air mixture; (2) preheating the fuel by the heated air stream. Of course it is important that no flame propagation occurs upstream of the combustor during engine operation at all flight regimes.

The availability of large hypersonic wind tunnels for full scale testing, and the availability of efficient computational fluid dynamic (CFD) codes can be utilized to study this problem. In fact, numerical solvers for full 3D Navier–Stokes equations in turbulent and reacting flows allow one to check the feasibility of the concept through parametric analyses and to reduce the need for quantitative numerical–experimental correlations.

Furthermore, the availability of new ultra high temperature ceramics (UHTC) materials that can withstand temperatures up to 3000 K allows one to find simpler solutions for the cowl at the different flight conditions without convective cooling and to improve the overall efficiency.

Hydrocarbon fuels are competitive with gaseous hydrogen for space vehicles [6] given their higher density. Operationally speaking, hydrocarbon fuels are much easier and safer to handle than hydrogen. Realistic ground testing can be accomplished in existing hypersonic plasma wind tunnels to simulate fully supersonic combustion mode at full scale and typical flight conditions.

However, the combustion of kerosene in the scramjet is complicated by long ignition times and reduced reaction rates, as compared to hydrogen. A recent experimental study on Kerosene injection on the inlet's conical surface of an axisymmetric scramjet model was carried out

by Vinogradov *et al*. [7]. This paper and the recent article by Guoskov *et al*. [8] suggest an investigation of the feasibility of this configuration.

In this paper a numerical study is performed for simple and relatively small axisymmetric scramjet configurations, including a conical forebody inlet with a cowl aligned with the free stream, a relatively short combustor and a nozzle, for flight Mach numbers $M = 6.5$ and 8. In this speed range a fixed geometry or a variable geometry with a small relative translation of the spike with respect to the cowl allows, in principle, to adapt to different Mach flight conditions.

EXPECTED PERFORMANCES OF SCRAMJET ENGINES FOR REUSABLE LAUNCH VEHICLES

Implementation of airbreathing propulsive devices for crossing the atmosphere seems to be the most logical solution to reduce the take-off to in-orbit payload mass ratio. Utilization of the oxygen in the atmosphere instead of carrying oxidizers on board results in a substantial improvement in the specific impulse. However some considerations are in order. The airbreathing engines generate a thrust (T) that is given by the ingested air mass flow rate ($\dot{m}$) multiplied by its specific momentum change ($\Delta V = V_e - V_\infty$); $T = \dot{m}\Delta V$. This thrust neglects a force resulting from the difference between the exit and the inlet pressure and assumes negligible fuel mass flow rate ($\dot{m}_f/\dot{m} \ll 1$).

On the other hand the energy addition ($\dot{E}$) to the air is related to the heat of combustion of the fuel with air (Q_f) and to its mass flow rate ($\dot{m}_f$). For an ideal situation, i.e. for a full conversion of all the chemical energy into internal energy and subsequently into kinetic energy, one gets

$$\dot{E} = \dot{m}_f Q_f = \frac{1}{2}(V_e^2 - V_\infty^2)\dot{m} = \frac{1}{2}\Delta V(V_e + V_\infty)\dot{m} = T\bar{V} \tag{1}$$

where

$$\bar{V} = \frac{V_\infty + V_e}{2} = V_\infty + \frac{\Delta V}{2} \tag{2}$$

The main performance parameter is the specific thrust, i.e. the thrust generated per unit fuel mass flow rate:

$$T_{sp} = \frac{T}{\dot{m}_f} = \frac{Q_f}{\bar{V}} = \frac{Q_f}{V_\infty + (\Delta V/2)} = \frac{Q_f}{V_\infty + T_{sp}(\dot{m}_f/2\dot{m})} \tag{3}$$

T_{sp} is proportional to the specific impulse I_{sp} by $T_{sp} = g_0 I_{sp}$, $g_0 = 9.81$ [m/s^2] being the reference acceleration of gravity.

Introducing the fuel mass ratio (for the case of kerosene $f_s \cong 0.06$):

$$f = \frac{\dot{m}_f}{\dot{m}} = \mathrm{ER}f_s \tag{4}$$

and substituting this into Equation (3) yields

$$T_{sp}^2 f + 2T_{sp}V_\infty - 2Q_f = 0 \tag{5}$$

that relates the specific thrust to the flight conditions and to the fuel heat of combustion:

$$T_{sp} = \frac{-V_\infty \pm \sqrt{V_\infty^2 + 2fQ_f}}{f} \tag{6}$$

$$\text{At low values of Mach } (2 \leqslant M_\infty \leqslant 3)\ V_\infty^2 \ll 2fQ_f, \text{ and } T_{sp} \cong \frac{\sqrt{2fQ_f} - V_\infty}{f} \tag{7}$$

$$\text{When the flight velocity is very high } (V_\infty^2 \gg 2fQ_f) T_{sp} \to \frac{Q_f}{V_\infty} \tag{8}$$

Equation (8) shows that, for a given value of the fuel heat of combustion with air (Q_f), the 'ideal' specific thrust evolves in the opposite way of the flight velocity.

Figure 1 shows the results of the calculations based on Equation (6), for Hydrogen ($Q_f = 1.2 \times 10^5$ kJ/kg), in the case ER = 1, and Kerosene ($Q_f = 4.3 \times 10^4$ kJ/kg) for different values of the fuel equivalence ratio ER. Figure 1 shows also the values of T_{sp} for Kerosene (at two values of the fuel equivalence ratio ER = 0.63, ER = 1) that have been computed (when combustion takes place in the engine) for the scramjet geometry and for the range of flight speeds considered in the present paper. The discrepancy with the values of the curves is due to the fact that the above equations are obtained with a simple global theoretical model in the ideal situation that the energy provided by the fuel combustion is completely converted into kinetic energy and do not include other losses caused by a number of possible sources

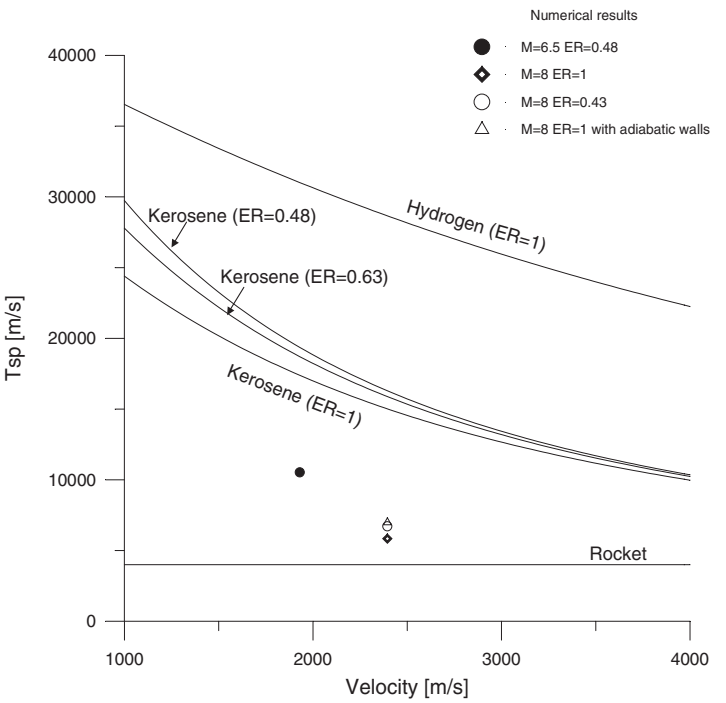

Figure 1. Specific thrust, comparison between Equation (6) and numerical results.

(energy exchanges with the walls, entropy production due to viscosity, thermal conductivity and species diffusion effects, total pressure losses related to the presence of shock waves and to turbulence, presence of unburned gases, chemical non-equilibrium, etc.).

Some of these phenomena have been taken into account in the numerical model developed in the next sections, based on full Navier–Stokes equations for turbulent and reacting flows.

AXISYMMETRIC SCRAMJET WITH UPSTREAM FUEL INJECTION

The geometry investigated consists of a relatively small axisymmetric scramjet configuration with a conical forebody inlet (about 45 cm), a cowl aligned with the free stream, a relatively short combustor (about 25 cm) and a nozzle (about 20 cm), see Figure 2. The spike is similar to the one of the axisymmetric scramjet engine developed by the Central Institute of Aviation Motors (CIAM) in Russia and investigated in flight tests from 1991 to 1998, see Reference [9]. The inlet geometry has been selected to ensure that, in the range of flight speeds and altitudes of interest, the shock formed at the tip of the cone reflects to the cowl (without spillage) to redirect the flow parallel to the combustor (and to the free stream). A small flap can be extended from the front of the cowl to adapt, in principle, the inlet geometry to lower Mach numbers. The engine includes a short constant-area isolator (with length of about

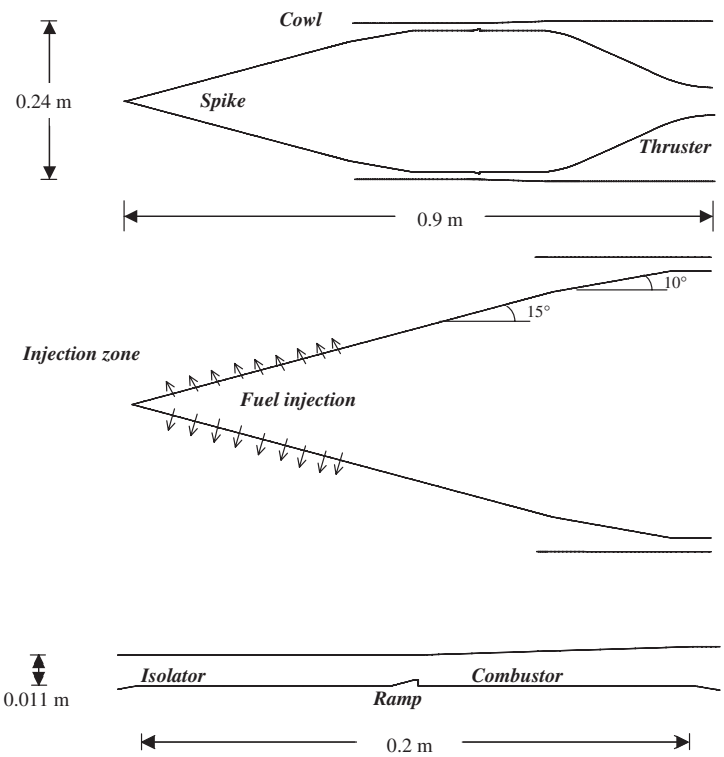

Figure 2. Scramjet geometry.

10 cm) located before a ramp that initiates ignition and eventually acts as a flame holder. The functions of the isolator are to prevent the shock train produced by the shocks reflection on the cowl and on the spike from entering the combustor (to ensure uniform conditions at the combustor entry) and to prevent shock waves (originated by combustion or by strong adverse pressure gradients) from traveling up through the inlet causing spillage and unstart [10, 11]. The combustor has a slightly diverging section to promote expansion during combustion and avoid choking.

The overall length of the isolator–combustor system is about 20 cm to minimize skin friction penalties.

The nozzle is a simple axisymmetric Bezier revolution surface that produces a continuous expansion. Different schemes have been investigated. The first one foresees fuel injection at the spike tip (see Figure 2). Alternatively, some of the fuel can be injected at the cowl tip. These schemes have been compared with the fuel injection in the combustor (e.g. axially from the backward facing step of the ramp). The ramp has been located in the combustor to promote fuel 'auto-ignition' as a consequence of the turbulent mixing and of the high temperature and pressure generated behind the shock wave at supersonic speeds.

It must be pointed out that the scramjet geometry and in particular the inlet, combustor and thrusters have been assumed as simple as possible for a preliminary check of the proposed idea. The optimization of each component and the integrated optimization of inlet/combustor/thrusters are outside the scope of the present work.

GOVERNING EQUATIONS AND NUMERICAL MODEL

The gas flowing in the scramjet engine has been modelled as a mixture of reacting gases in thermal and chemical non-equilibrium, so the equations considered are the balance equations for mass, chemical species, momentum and total energy. They are written as follows:

Continuity:

$$\frac{\partial \rho}{\partial t} + \underline{\nabla} \cdot (\rho \underline{V}) = 0 \tag{9}$$

Species:

$$\frac{\partial (\rho m_i)}{\partial t} + \underline{\nabla} \cdot (\rho \underline{V} m_i) + \underline{\nabla} \cdot \underline{J}_i = \dot{\omega}_i \tag{10}$$

Momentum:

$$\frac{\partial (\rho \underline{V})}{\partial t} + \underline{\nabla} \cdot (\rho \underline{V}\,\underline{V}) + \underline{\nabla} p = 2\underline{\nabla} \cdot [\mu (\underline{\nabla V})_0^{\mathrm{s}}] \tag{11}$$

where

$$(\underline{\nabla V})_0^{\mathrm{s}} = \frac{1}{2}((\underline{\nabla V}) + (\underline{\nabla V})^{\mathrm{T}}) - \frac{1}{3}(\underline{\nabla} \cdot \underline{V})\underline{\underline{U}} \tag{12}$$

Energy:

$$\frac{\partial (\rho E)}{\partial t} + \underline{\nabla} \cdot [(\rho E + p)\underline{V}] = \underline{\nabla} \cdot \left(\lambda \nabla \vartheta + 2\mu (\underline{\nabla V})_0^{\mathrm{s}} \cdot \underline{V} + \sum_i h_i \underline{J}_i \right) - \sum_i h_i \dot{\omega}_i \tag{13}$$

The free stream is composed by air; kerosene can be injected at different locations and the fuel-oxygen mixture undergoes the overall chemical reaction

$$4C_{12}H_{23} + 71O_2 = 48CO_2 + 46H_2O \tag{14}$$

Therefore the gas is in general modelled as a mixture with 79% of molecular nitrogen plus four chemical reacting species: kerosene, carbon dioxide, water, molecular oxygen.

Using the simple one-step equation (14) for the combustion chemistry is a rather strong simplification for the non-equilibrium chemical modelling that allows one to obtain useful results from the numerical simulations, but it is not completely adequate for a proper hydrocarbon combustion model, especially to predict pre-ignition, boundary layer combustion and to take into account coupling between chemical reactions and turbulence. These complex aspects are out of the scope of the present paper.

For each species the perfect gas model applies and the Dalton's law is applicable:

$$p = \sum_i p_i \tag{15}$$

where the summation is extended to all the species considered. As a consequence, the following relation holds:

$$\rho = \frac{p}{R_0 \vartheta \sum_i m_i/\Gamma_i} \tag{16}$$

The internal energy of the mixture is defined as

$$e = \sum_i (m_i e_i) \tag{17}$$

where e_i, the internal energy of the single component gas, is the sum of the energies representing the different degrees of the freedom of the molecules (translational, rotational, vibrational and electronic modes are in equilibrium at the temperature θ).

From these expressions the specific enthalpy for each species may be calculated as

$$h_i = e_i + R_i \theta \tag{18}$$

Computation of the diffusive fluxes requires knowledge of the transport coefficients. For pure species, the following expressions are derived from the kinetic theory of gases [12]:

Viscosity:

$$\mu_i = \frac{2.6693 \times 10^{-6} \sqrt{\Gamma_i \vartheta}}{\sigma_i^2 \Omega_{\mu i}} \tag{19}$$

Thermal conductivity:

$$\lambda_i = \frac{15}{4} \left(\frac{\mu_i R_0}{\Gamma_i} \right) \left(\frac{4}{15} \frac{c_{pi} \Gamma_i}{R_0} + \frac{1}{3} \right) \tag{20}$$

Mass diffusivity:

$$D_{ij} = \frac{0.0188 \cdot \vartheta^{3/2} \sqrt{(\Gamma_i + \Gamma_j)/\Gamma_i \Gamma_j}}{p \sigma_{ij}^2 \Omega_{Dij}} \tag{21}$$

When one considers the global transport properties of the mixture, semi-empirical rules may be applied, such as Wilke's rule for viscosity and thermal conductivity:

$$\mu, \lambda = \frac{\sum_i \chi_i(\mu_i, \lambda_i)}{\sum_j \chi_j \left[\frac{1}{\sqrt{8}}(1 + M_i/M_j)^{1/2}(1 + ((\mu_i, \lambda_i)/(\mu_j, \lambda_j))^{1/2}(M_j/M_i)^{1/4})^2\right]} \tag{22}$$

For the diffusion coefficient of the species i in the mixture, the following relation may be applied:

$$D_i = \frac{1 - \chi_i}{\sum_j (\chi_j/D_{i,j})} \tag{23}$$

The chemical production rate of species i in the generic reaction k is

$$\dot{\omega}_{ik} = \Gamma(\nu''_{ik} - \nu'_{ik}) \cdot \left[K_{\mathrm{fk}} \prod_j C_j^{\nu'_{jk}} - K_{\mathrm{bk}} \prod_j C_j^{\nu''_{jk}}\right] \tag{24}$$

where K_{fk} and K_{bk} are the forward and backward rate constants for the kth reaction, modelled according to the Arrhenius law:

$$K_k = A_K \theta^{\beta_K} \exp\left(-\frac{E_k}{R_0 \vartheta}\right) \tag{25}$$

The following values have been considered for the constants appearing in the Arrhenius law for the forward reaction ($A_k = 2.587 \times 10^9$; $E_k = 1.256 \times 10^8$ [J/kgmol]; $\beta_k = 0$).

The constants for the backward reaction are computed from the equilibrium constant.

The source term for species i appearing in the species balance equations is then written as

$$\dot{\omega}_i = \Gamma_i \sum_k \dot{\omega}_{ik} \tag{26}$$

All the computations were performed assuming that the scramjet walls are maintained at a constant temperature of 1000 K.

Species boundary conditions on the walls have been assigned under the assumption of a noncatalytic wall, i.e. the diffusive flux of atoms at the wall is set to zero.

The field equations have been solved by a numerical program based on a finite volumes method that deals with a general system of partial differential equations in the general form:

$$\frac{\partial \tilde{U}}{\partial t} + \frac{1}{V} \sum_i (\bar{\underline{F}} - \bar{\underline{G}})_i \cdot \underline{A}_i = \tilde{H} \tag{27}$$

Turbulence has been modelled with the standard k–ε formulation.

Non-dissipative fluxes are computed according to the flux difference splitting technique proposed by Roe [13]. Dissipative fluxes are computed by the Gauss theorem. Accuracy is second order in space. Time integration is performed by an explicit multi-stage Runge–Kutta scheme. Multigrid techniques are used to accelerate convergence.

Generally, accurate computations of the gradients appearing in the field equations require structured grids, which have been used for all computations in the present work. The computation of the heat transfer or of the skin friction requires detailed resolution of the flow

very near the surface. An iterative approach was followed to determine the near-body grid resolution, which gives the grid-solution independence. In our computations, the value of the grid spacing near the wall was found to be 10^{-6} (m). Grid refinement in strong gradient regions was made when necessary through a solution adaptive approach.

RESULTS AND DISCUSSION

Fluid-dynamic field in the scramjet engine

When fuel is injected into the scramjet, it undergoes turbulent mixing with the air and, if the chemical reaction (14) is included in the numerical model, it 'auto-ignites' due to the high temperature and pressure behind the shock wave formed at the ramp. The flight conditions investigated refer to a typical flight corridor for transatmospheric trajectories. In particular, two conditions have been selected: (1) $M = 6.5$, $z = 20$ km; (2) $M = 8$, $z = 25$ km.

Plates 1 and 2 show the contours of the static pressure and of the Mach number along the engine (in the inlet, in the combustor and in the nozzle) for the case $M = 6.5$ and $z = 20$ km, when no fuel is injected. The corresponding contours of the temperature in the isolator and combustor are shown in Plate 3. Free-stream air entering the scramjet is first compressed by oblique shocks formed at the conical forebody tip and then reflected on the internal cowl. In particular, the oblique shock wave produced at the spike tip is reflected at the cowl and then subsequently reflected near the isolator entrance. It is also evident that the interaction of the shock reflected at the cowl with the Prandlt–Meyer expansion fan originated at the end of the conical axisymmetric spike. At the isolator entrance, the Mach number is about 3, the pressure is of the order of magnitude of 1 atmosphere, and the temperature is about 750 K. When the supersonic flow reaches the ramp located in the combustor, a shock wave is formed that further increases the temperature and the pressure and decreases the local Mach number.

In Plates 4–6 the case without injection (upper part of plates) is compared with the case in which Kerosene is injected at the spike tip at a temperature of 450 K (lower part of plates).

The mass flow rate of the injected kerosene fuel has been assigned on the basis of the fuel/air stoichiometric ratio ($f = 0.06$, corresponding to an equivalence ratio $\mathrm{ER} = 1$) and on the basis of the total mass flow rate of the air within the inlet. For a fuel equivalence ratio $\mathrm{ER} = 1$, in the case $M = 6.5$, $z = 20$ km, the fuel flow rate is 0.44 kg/s, whereas in the case $M = 8$, $z = 25$ km the fuel flow rate is 0.26 kg/s. The fuelled results shown in Plates 4–6 correspond to $M = 6.5$, $z = 20$ km and to a value of the equivalence ratio $\mathrm{ER} = 0.63$.

When kerosene is injected along the spike, the strength of the oblique shock formed at the spike tip increases, so that the reflection point at the cowl surface moves upstream and increases the pressure at the entry of the isolator. A rather uniform filling of cross section, especially in the region close to the wall occurs at the exit of the inlet as confirmed by Plate 7(a,b) where the contours of the Kerosene mass fraction are compared in the two cases: (a) fuel injection at the spike tip; (b) fuel injection at the base of the ramp located in the combustor. When fuel is axially injected from the base of the step, Kerosene flows close to the combustor wall (Plate 7(b)).

The improved mixing efficiency in the configuration with fuel injection at the spike tip, compared to the axial injection in the combustor, is also illustrated in Figure 3, where the profile of Kerosene mass flux is shown in a cross section of the combustor ($x = 0.54$ m) for

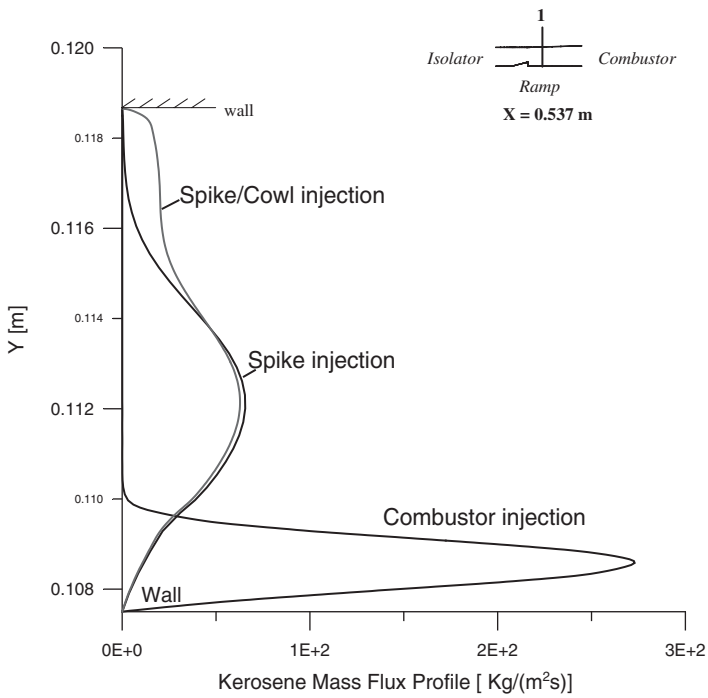

Figure 3. Kerosene mass flux profile in the case $M_\infty = 6.5$, $z = 20\,\text{km}$, $\text{ER} = 0.55$ at station $x = 0.54\,\text{m}$.

different fuel injection modes. In particular, mixing efficiency is further increased if Kerosene is simultaneously injected along the spike (80%) and at the cowl surface (20%).

It must be pointed out that fuel injection along the spike not only improves mixing efficiency, as discussed above, but also increases the temperature of the fuel/air mixture thus promoting ignition and combustion.

Plate 8 shows the contours of the Kerosene mass fraction for the same conditions of Figure 3, when combustion of the fuel–air mixture takes place. In particular, for upstream fuel injection spontaneous ignition and combustion occurs and a negligible fraction of unburned kerosene is found at the scramjet exit. On the contrary, in the case of axial fuel injection at the ramp base, the fuel remains completely unburned, even if the temperature and pressure are initially 'artificially' increased in the numerical model of the combustor.

Plates 9–13 refer to the case of supersonic combustion at the same conditions of Plate 7(a) ($M = 6.5$, $z = 20\,\text{km}$, fuel injection at the spike tip and $\text{ER} = 0.63$).

The temperature contours (Plate 9), the Mach number contours (Plate 10) and the contours of static pressure (Plate 11) are compared in the two cases: (a) only fuel injection without combustion; (b) combustion.

The numerical results corresponding to the case of fuel injection without combustion are obtained assuming, in the numerical code, a non-reacting mixture.

In particular Plate 11 shows a large pressure increase in the combustor and Plate 12 shows that, when the combustion of the fuel–air mixture takes place, a significant mass fraction of

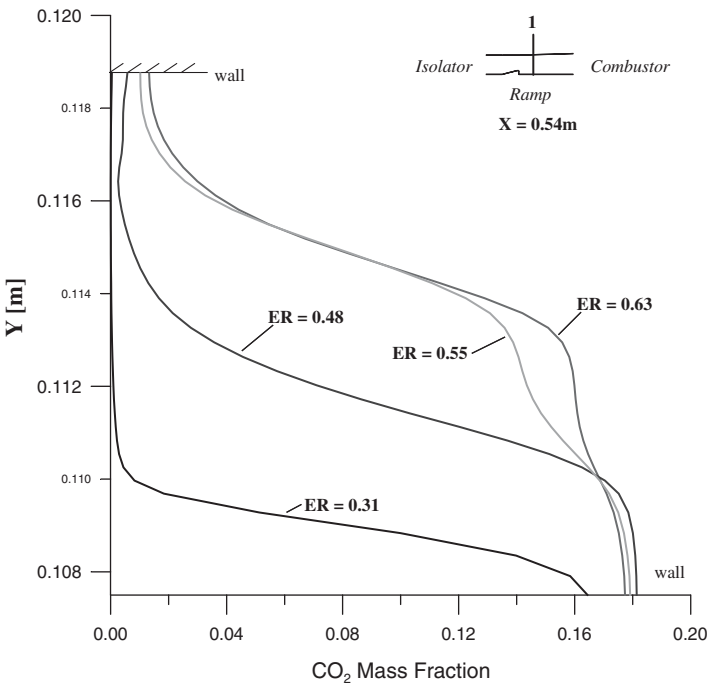

Figure 4. CO_2 mass fraction comparison for different ER in the case $M_\infty = 6.5,\ z = 20\,\text{km}$, at the station $x = 0.54\,\text{m}$.

CO_2 is formed as a product of the reaction process. In this case no unburned kerosene was found at the scramjet exit.

The high enthalpy products created by combustion are expanded in the nozzle to a velocity and pressure greater than the free-stream.

In Plate 13 the contours of the velocity magnitude in the nozzle are compared for the combusting and non-combusting cases. Higher velocities are reached when combustion occurs (order of magnitude of 2000 m/s), resulting in a positive net specific thrust.

Figure 4 shows the effect of the fuel equivalence ratio ER on the CO_2 mass fraction in the combustor cross-section at $x = 0.54\,\text{m}$. Increasing ER from 0.31 to 0.63, the CO_2 mass fraction increases and the combustion takes place in a larger part of the cross-section.

The pressure distributions along the walls of the entire scramjet are shown in Figures 5 and 6, in the cases $M = 6.5,\ z = 20\,\text{km}$ ($\text{ER} = 0$, $\text{ER} = 0.31$ and $\text{ER} = 0.63$) and $M = 8,\ z = 25\,\text{km}$ ($\text{ER} = 0,\ \text{ER} = 0.43,\ \text{ER} = 1$). The heat addition due to Kerosene burning results in a large peak of pressure in the combustor that produces a positive thrust.

Thrust evaluation

The net thrust developed by the scramjet is the overall force acting on the engine. This can arbitrarily divided into a 'propulsive' force generated by the expansion of the exhaust gases (at the aft section of the engine) and a 'drag' on the engine.

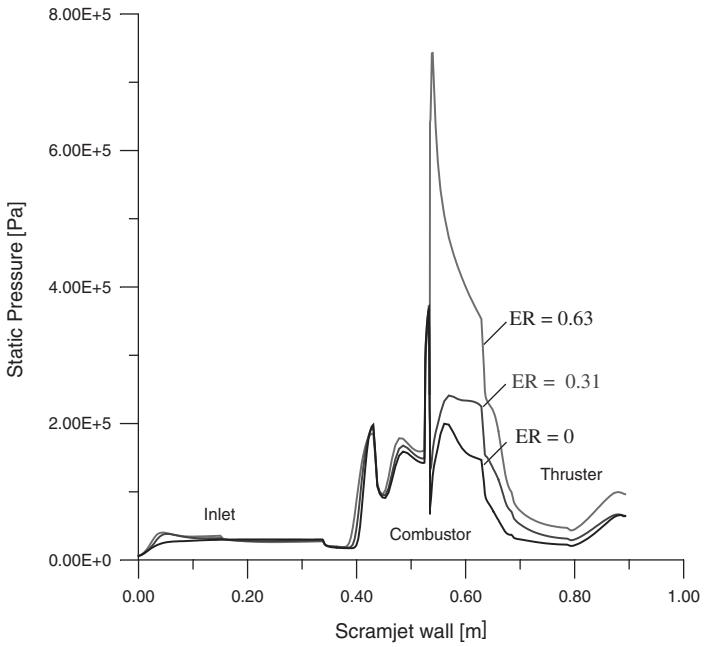

Figure 5. Pressure distribution on the internal scramjet walls at $M = 6.5$, $z = 20$ km, comparison between different ER.

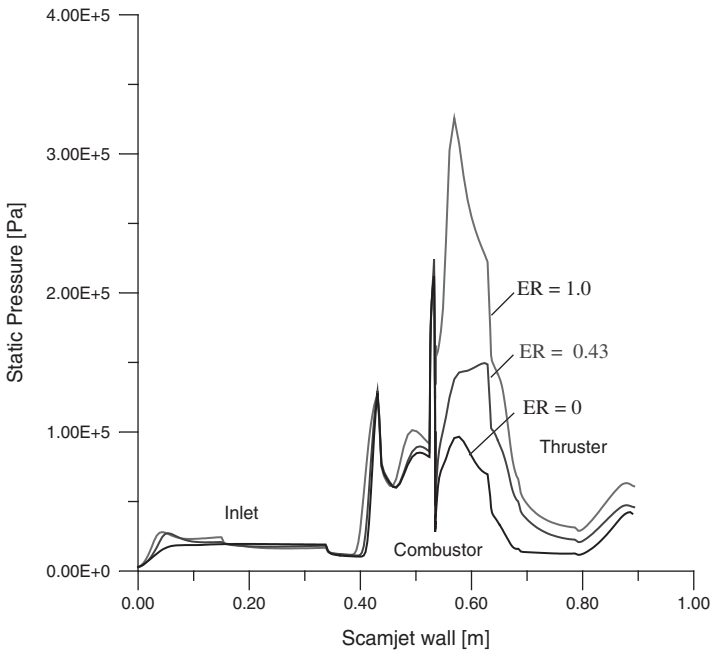

Figure 6. Pressure distribution on the internal scramjet walls at $M = 8$, $z = 25$ km, comparison between different ER.

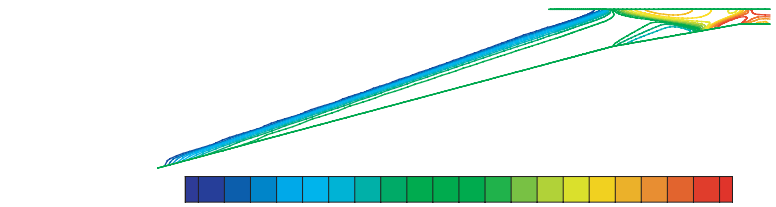

Inlet

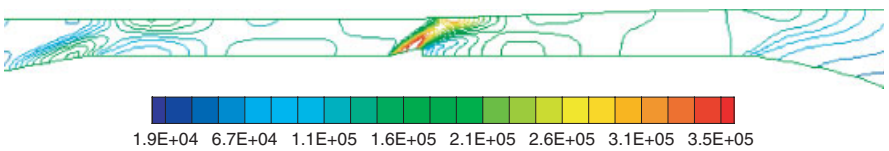

Combustor

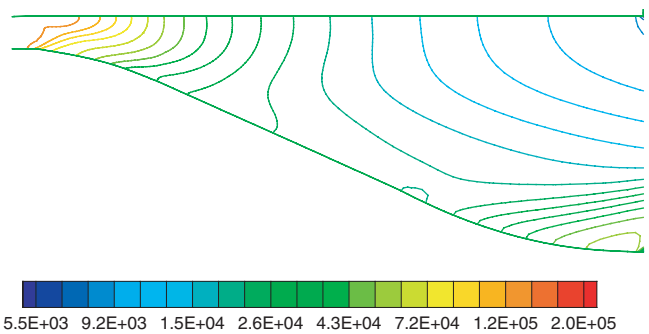

Nozzle

Plate 1. Contours of static pressure (Pa) in the case $M_\infty = 6.5,\ z = 20\,\text{km},\ \text{ER} = 0$.

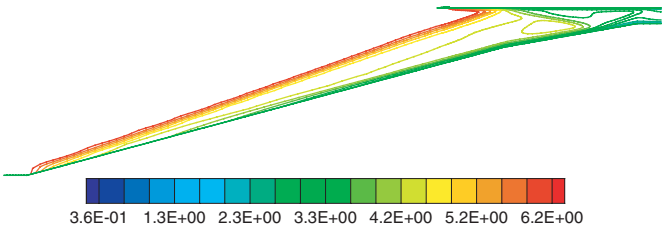

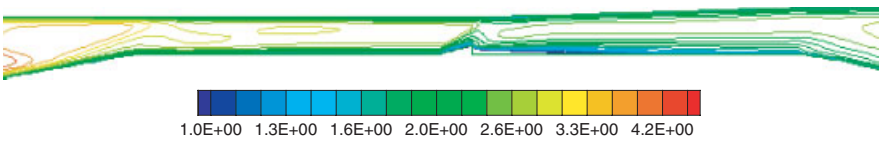

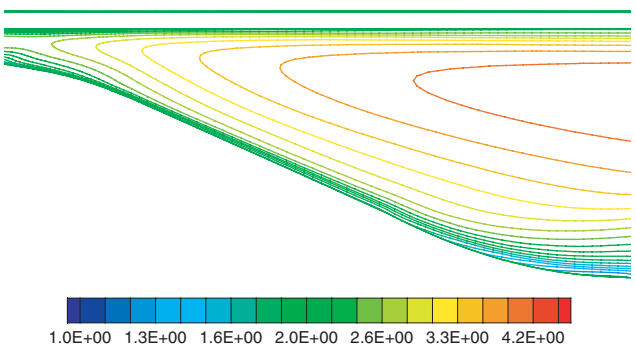

Plate 2. Contours of Mach number in the case $M_\infty = 6.5,\ z = 20\,\text{km},\ \text{ER} = 0$.

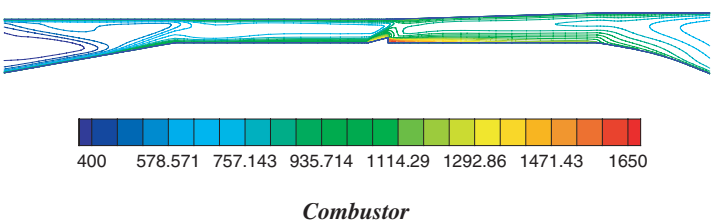

Plate 3. Contours of temperature (K) in the case $M_\infty = 6.5,\ z = 20\,\text{km},\ \text{ER} = 0$.

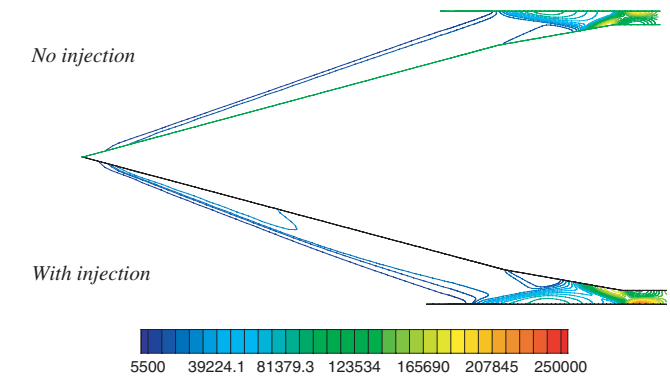

Plate 4. Contours of static pressure (Pa) in the case $M_\infty = 6.5$, $z = 20$ km, comparison between the case ER $= 0$ and 0.63.

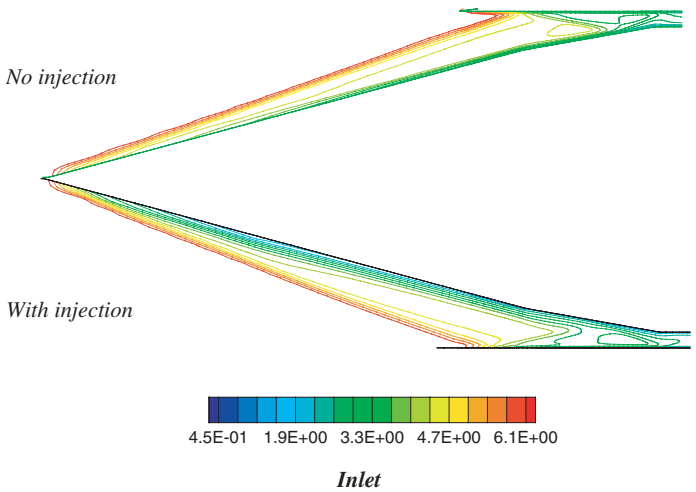

Plate 5. Contours of Mach number in the case $M_\infty = 6.5$, $z = 20$ km, comparison between the case ER $= 0$ and 0.63.

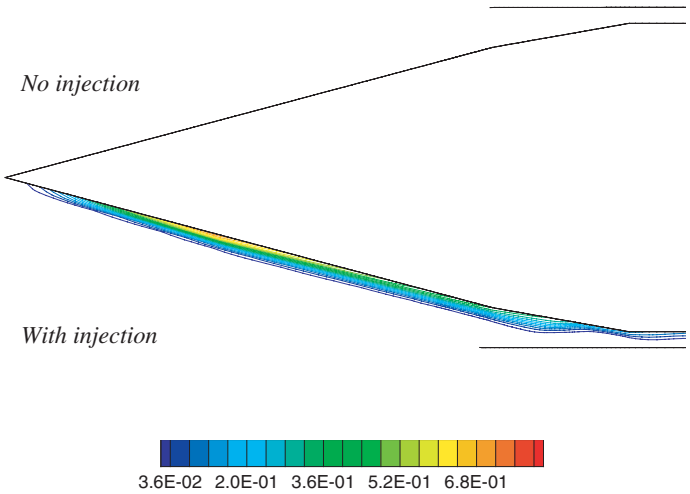

Plate 6. Contours of $C_{12}H_{23}$ Mass fraction in the case $M_\infty = 6.5$, $z = 20$ km, comparison between the cases ER = 0 and 0.63.

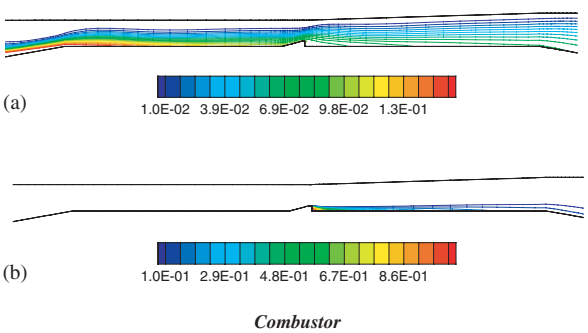

Plate 7. Contours of $C_{12}H_{23}$ Mass fraction (ER = 0.63) in the case $M_\infty = 6.5$, $z = 20$ km, comparison between the cases of spike-injection (a) and ramp-injection (b).

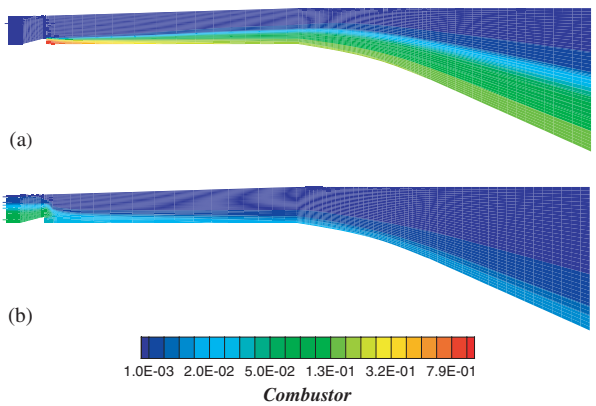

Plate 8. Contours of Kerosene mass fraction in the case $M_\infty = 6.5$, $z = 20$ km, ER $= 0.55$. Comparison between the cases of ramp-injection (a) and spike-injection (b).

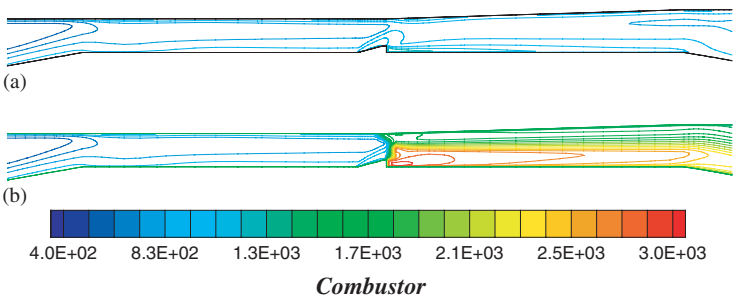

Plate 9. Temperature contours (K) in the case $M_\infty = 6.5$, $z = 20$ km, comparison between the cases without combustion (a) and with combustion (ER $= 0.63$) (b).

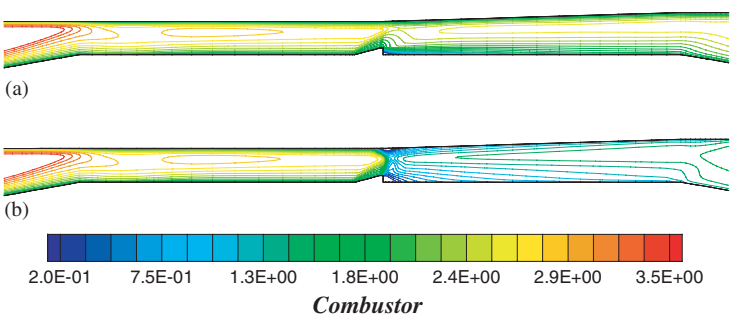

Plate 10. Contours of Mach number in the case $M_\infty = 6.5$, $z = 20$ km, comparison between the cases without combustion (a) and with combustion (ER $= 0.63$) (b).

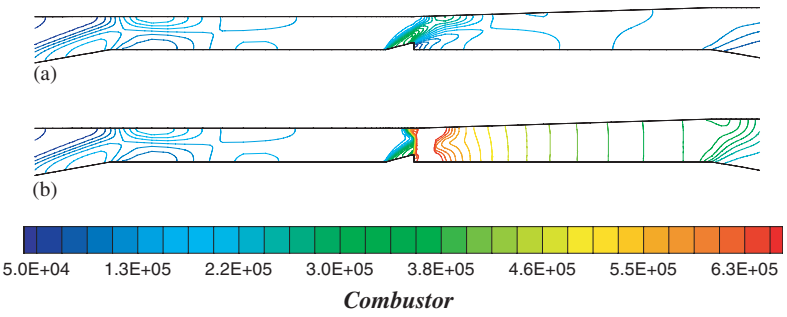

Plate 11. Contours of static pressure in the case $M_\infty = 6.5$, $z = 20$ km, comparison between the cases without combustion (a) and with combustion (ER = 0.63) (b).

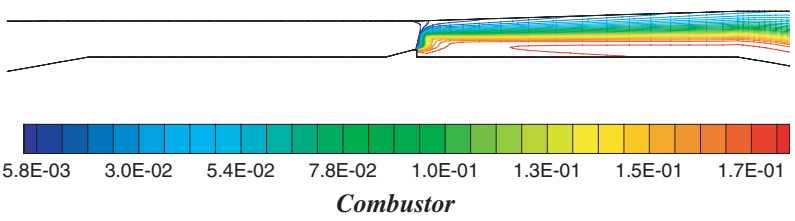

Plate 12. Contours of CO_2 mass fraction (ER = 0.63) in the case $M_\infty = 6.5$, $z = 20$ km.

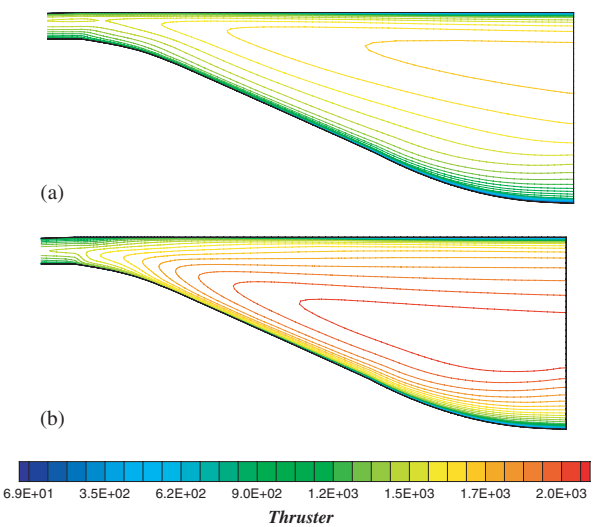

Plate 13. Contours of velocity magnitude (m/s) in the case $M_\infty = 6.5$, $z = 20$ km, comparison between the cases without combustion (a) and with combustion (b) (ER = 0.63).

Table Ia. Computed forces in the case $M_\infty = 6.5,\ z = 20\,\text{km}$.

$M_\infty = 6.5$								
	0		0.48		0.55		0.63	
ER	(a)	(b)	(a)	(b)	(a)	(b)	(a)	(b)
Spike	−1389.7	−157.6	−1504.1	−108.4	−1520.7	−103.9	−1537.5	−99.6
Cowl	3.9	−175.6	4.3	−195.4	4.3	−198.3	4.4	−200.8
Combustor	8.4	−489.2	1185.6	−534.3	1347.9	−538	1488	−551.7
Thruster	1207.6	−191.5	2692	−289.5	2858	−297.2	3004.3	−306.3
Thrust T(N)	0		2315.1		2617.1		2846.5	
Specific thrust T_{sp}(m/s)	/		10523.2		10223		9815.5	
Net force T_n(N)	−1183.7		1250.2		1552.1		1800.8	

(a) Pressure force (N).
(b) Viscous force (N).

Table Ib. Computed forces in the case $M_\infty = 8,\ z = 25\,\text{km}$.

$M_\infty = 8$						
	0		0.43		1	
ER	(a)	(b)	(a)	(b)	(a)	(b)
Spike	−788.9	−124.7	−829.2	−93.4	−917.7	−71.2
Cowl	2.4	−136.9	2.6	−156.9	2.8	−176.6
Combustor	−37.4	−378.9	105.5	−410	537.4	−459.7
					621.3*	−408.3*
Thruster	589.1	−140.7	1417	−204.7	1969	−245.2
					2106.5*	−219.8*
Thrust T(N)	0		737.9		1516.9	
					1815.1*	
Specific thrust T_{sp}(m/s)	/		6708.2		5834.2	
					6981.2*	
Net force T_n(N)	−1016		−161.9		638.8	
					937*	

(a) Pressure force (N).
(b) Viscous force (N).
*Adiabatic walls.

A summary of the axial forces applied to the engine components, for the different conditions investigated, is given in Table I.

The different contributions include pressure and viscous forces along the spike, the cowl, the combustor and the nozzle. Negative and positive forces indicate a drag and a thrust, respectively.

Obviously, the total axial force is negative (a drag) for zero or low values of the fuel equivalence ratio. When the amount of injected and burned fuel is relatively high (high

equivalence ratio), the energy provided to the stream by the combustion produces a positive net thrust.

Table I shows, for the different conditions, the overall thrust T (i.e. the overall axial force plus the aerodynamic drag), the specific thrust (T_{sp}) and the net thrust $T_n = T - D$ (i.e. the resulting accelerating force). The drag of the engine is assumed to be the total force acting on the structure for no fuel injection (ER = 0).

In Figure 1 some computed values of the specific thrust (T_{sp}) are reported and compared to the results of Equations (6). In particular, the numerical results refer to the case ER = 0.48 (for $M = 6.5$) and ER = 1 ($M = 6.5$, 8). The lower values of the computed specific net thrust, compared to the theoretical predictions based on Equation (6), show that energy losses are present that are not taken into account in Equation (6) even if the losses are reduced in the case of adiabatic walls. The numerical results confirm the general trend predicted by the theoretical predictions (smaller specific net thrust at higher velocities).

Thermal issues

The heat flux distribution at the wall and the integrated surface heat flux have been computed along the different scramjet components (spike, combustor, nozzle) for the different conditions investigated. Some of these results are summarized in Table II. As discussed before, the computations have been carried out assuming that the scramjet walls are convectively cooled and maintained at a constant temperature of 1000 K.

Table II shows that the worst conditions, in terms of thermal load (integrated heat flux along the wall), occur at the combustor, when fuel is burned. In particular, the integrated heat flux at the cowl, combustor and thrusters walls increases with ER. On the contrary, the thermal load on the spike is a decreasing function of the fuel equivalence ratio.

In fact, high values of the heat flux occur at the spike and at the cowl leading edge (even in the absence of combustion). The worst conditions occur at high Mach numbers without fuel injection. In this case the maximum values of the computed heat fluxes at the spike tip and at the cowl leading edge are of the order of $10^6\,W/m^2$, that correspond to an equilibrium radiation temperature of about 2000 K.

Fuel injection at the spike tip is beneficial because fuel is injected at a lower temperature (450 K) thus reducing the heat flux at the spike and at the cowl leading edge. This seems to be an additional advantage of the scheme of scramjet with upstream fuel injection.

When combustion takes place, the total temperature in the combustor is higher but does not exceed 3000 K.

The above results suggest to employ advanced materials for thermal protection of the spike tip, of the cowl leading edge and of the combustor walls. The so-called ultra high temperature ceramics (UHTC) materials, like Titanium diboride, Zirconium diboride and Hafnium diboride, that can withstand temperatures up to 3000 K in the presence of reacting gas mixtures seem to offer simpler solutions at the different flight conditions without (or with partial) convective cooling. In particular, decreasing the cooling at the combustor walls (and therefore increasing the wall temperature up to a temperature of the order of the total temperature of the gas mixture) a larger net thrust is expected due to the smaller energy losses caused by the heat transfer through the combustor walls.

Numerical computations have been carried out in the ideal case of adiabatic combustor walls, for $M = 8$, $z = 25\,km$, ER = 1. The maximum value of the computed temperature at the

Table IIa. Computed heat fluxes in the case $M_\infty = 6.5,\ z = 20\,\text{km}$.

	$M_\infty = 6.5$ Integrated heat flux $\times 10^4$ (W)			
ER	0.31	0.48	0.55	0.63
Spike	4	1.7	0.8	0.02
Cowl	11	11.3	11.5	11.7
Combustor	53.8	82.6	83.8	87.9
Thruster	23	34.9	37	39.1
Total integrated heat flux	91.8	130.5	133.1	138.7

Table IIb. Computed heat fluxes in the case $M_\infty = 8,\ z = 25\,\text{km}$.

	$M_\infty = 8$ Integrated heat flux $\times 10^4$ (W)	
ER	0.43	1
Spike	6.3	1.6
Cowl	15.3	16.9
Combustor	64.1	89.3
Thruster	29.6	40.5
Total integrated heat flux	115.3	148.3

wall is in fact of the order of the total temperature (about 3000 K). In this case, as shown in Table Ib, the net force on the scramjet is about 50% higher than in the case of a wall convectively cooled at a constant temperature of 1000 K (even though regenerative cooling will limit this improvement).

CONCLUSIONS

A scramjet configuration for airbreathing engines that use hydrocarbon fuels injected at the spike tip has been investigated. A numerical analysis has been carried out assuming that the scramjet engine is used on a reusable launch vehicle accelerating through the atmosphere along a typical ascending trajectory at constant dynamic pressure, for different fuel equivalence ratios.

The numerical results prove the feasibility of the proposed scheme and show a number of advantages, in particular an improved mixing and combustion efficiency resulting in large propulsive forces in a limited size combustor and in reduced thermal loads.

The optimization of the inlet, isolator, combustor and nozzle geometries requires deeper numerical and experimental analysis, to solve a number of practical problems, including those related to low Mach number operation and thermal choking (not addressed in the present work). During the study, the best location for the fuel injection should also be investigated.

NOMENCLATURE

c_p	specific heat at constant pressure (J/kg/K)
D	mass diffusivity (m^2/s)
e	internal specific energy (J/kg)
E	total specific energy (J/kg)
ER	equivalence ratio
f	fuel mass ratio ($f = \frac{\dot{m}_f}{\dot{m}} = \mathrm{ER} f_s$)
h	specific enthalpy (J/kg)
J_i	diffusive mass flux of species i ($kg/m^2/s$)
M	Mach number
$\dot{m}$	mass flow rate (kg/s)
m_i	mass fraction of species i
p	pressure (Pa)
Q_f	heat of combustion (J/kg)
R_0	universal constant ($R_0 = 8314.51$ J/K kgmol)
R_i	gas constant (J/kg/K)
T	thrust (N)
t	time (s)
T_{sp}	specific thrust (m/s)
V	velocity magnitude (m/s)
z	altitude (km)

Greek symbols

$\dot{\omega}_i$	reaction rate of species i ($kg/m^3/s$)
Γ_i	molecular weight of species i (kg/kgmol)
λ	thermal conductivity (W/m/K)
μ	viscosity (kg/m/s)
ν''_{ik}, ν'_{ik}	stoichiometric coefficients of species i in the kth reaction
θ	temperature (K)
ρ	density (kg/m^3)

Subscripts

e	exit
f	fuel
∞	ambient conditions
i	ith species
k	kth reaction
s	stoichiometric value

REFERENCES

1. Curran E. Scramjet engines: the first forty years. *Journal of Propulsion and Power* 2001; **17**(6):1138–1148.
2. Ferri A. Discussion on M. Roy's paper propulsion supersonique par turboreacteurs et par statoreacteurs. *Advances in Aeronautical Sciences*, vol. 1. Pergamon: Oxford, England, UK, 1959; 79–112.

3. Seiner JM, Dash SM, Kenzakovich DC. Historical survey on enhanced mixing in scramjet engines. *Journal of Propulsion and Power* 2001; **17**(6):1273–2386.
4. Scherrer D. Supersonic combustion. *Lecture Series 1998-01 in High Speed Propulsion*. Von Karman Institute for Fluid Dynamics, 26–29 January, 1998.
5. Monti R. Some considerations on supersonic combustion ram jets. *Vth European Aeronautical Congress*, 12–15 September, 1962.
6. Powell OA, Edwards JT, Norris RB, Numbers KE, Pearce JA. Development of hydrocarbon-fueled scramjet engines: the hypersonic technology (HyTech) program. *Journal of Propulsion and Power* 2001; **17**(6):1170–1176.
7. Vinogradov VA, Kobigsky SA, Petrov MD. Experimental investigation of kerosene fuel combustion in supersonic flow. *Journal of Propulsion and Power* 1995; **11**(1):130–134.
8. Guoskov OV, Kopchenov VI, Lomkov KE, Vinogradov VA. Numerical research of gaseous fuel preinjection in hypersonic three-dimensional inlet. *Journal of Propulsion and Power* 2001; **17**(6):1162–1169.
9. Rudakov A, Kopchenov V, Bezgin L, Guskov O, Lomkov K, Prokhorov A. Researches of hypersonic propulsion in central institute of aviation motors. *ESA SP-487*, 2002; 81–92.
10. Billing FS. Research on supersonic combustion. *Journal of Propulsion and Power* 1993; **9**(4):499–514.
11. Curran E, Heiser W, Pratt DT. Fluid phenomena in scramjet combustion. *Annual Review of Fluid Mechanics* 1996; **28**:323–360.
12. Hirchfelder JO, Curtiss CF, Bird RB. *Molecular Theory of Gases and Liquids*. Wiley: New York, 1954; 75–106.
13. Roe PL. Characteristic based schemes for the Euler equations. *Annual Review of Fluid Mechanics* 1986; **18**:337–365.

